Canonical Structures in Admissibility Space

Persistence Geometry and Empirical Basin Occupancy Across Physical Systems

UNNS Substrate Research Program

Synthesis Manuscript · Version 1.0 · 2026

Instruments: STRUC-I v1.0.4 · STRUC-PERC-I v2.5.0 · CLE v2.0.0 · PASP Field Generator

Corpora: helium (QM-I/Zeeman, 12 encodings) · 69 oxide ladders · neutrino detector (TMVA, DeepL, 67 encodings)

Planck CMB (TT/TE/EE) · protein MSM · Voyager 1 heliospheric transit (3,500 evaluations)

Adversarial corpus: 650 ladders (uniform, Pareto, randomwalk, shuffle) · hierarchical falsification complete

Total evaluations: $>14{,}000$ across >14 physical domains

Epistemic status. Part I (Sections 1–5) is theoretical synthesis grounded in the PASP/CLE v2.0.0 corpus. Part II (Sections 6–10) presents empirical domain analyses with fully operational pipeline outputs. Part III (Sections 11–13) combines the hierarchical falsification results with the dynamics frontier. Open theoretical problems are marked **[Open]**.

Abstract

We present a unified account of canonical structures in admissibility space, integrating the persistence geometry of the PASP/CLE v2.0.0 pipeline with empirical basin-occupancy measurements across four physical domains (helium spectroscopy, Planck CMB power spectra, neutrino detector distributions, and Voyager 1 heliospheric transit).

Central claim. What matters is persistence under deformation, not static encoding quality. Structural coherence is a persistence property measured over deformation fields in fundamental-constant space. Physically unrelated systems occupy the same admissibility basins because the geometry of $\mathcal{M}_{\text{adm}}$ constrains realizability universally, not because the systems share any physical law.

The manuscript establishes: (i) a complete formalization of persistence geometry, turbulence, manifold descriptors, and canonical lifts; (ii) domain-by-domain empirical occupancy measurements with rigidity class assignments; (iii) a cross-domain basin co-occupancy analysis replacing the weaker notion of "structural universality"; (iv) the Adversarial Locality Principle: fragmented manifolds admit local adversarial overlap by geometric necessity; (v) hierarchical falsification results over a 650-ladder adversarial corpus — five domains pass with zero adversarial penetration.

The similarity between helium and CMB at 0.993 is not a claim about physical connection. It is a claim about shared basin geometry: both systems reside in the Type-I dense interior of $\mathcal{M}_{\text{adm}}$, far from the admissibility boundary, with no mechanism for escape under the tested deformation envelope.

Contents

Part I
Foundations: Geometry of Admissibility Space

1 Canonicality, Admissibility, and the Structural Object

1.1 The problem of structural comparison

Physical systems are conventionally compared through domain-specific languages: quantum numbers and transition rules in spectroscopy, cross-sections and detector efficiencies in particle physics, angular power spectra in cosmology, plasma parameters in heliospheric science. These languages are precise within their domains. They do not provide a natural basis for comparison *across* domains.

This manuscript proposes and operationalizes an alternative comparison: *admissibility geometry*. Instead of asking what physical law governs a system, we ask what region of admissibility space its canonical encoding occupies, how deeply its persistence manifold extends into that region, and how resistant that manifold is to deformation. These questions have operational answers that are independent of physical interpretation.

1.2 The structural object: canonical gap-field ladders

Let $L = (L_1, \ldots, L_n)$ be a ladder encoding — an ordered sequence of scalar values extracted from a physical system by a domain adapter. The *canonicalization* of L is the sequence L_{can} obtained by sorting ascending, removing non-finite values, and deduplicating. The *gap field* is $\Delta_i = L_{i+1} - L_i$ for $i = 1, \ldots, n-1$.

All downstream structural analysis operates on Δ, not on L directly. This makes the analysis dimensionless up to a scaling factor absorbed into the normalized κ parameter, enabling cross-domain comparison without dimensional conversion.

1.3 The admissibility manifold

Definition 1.1 (Vulnerability graph and admissibility)**.** For scale parameter $\kappa \geq 0$, the vulnerability graph $G_\kappa(L)$ has vertex set $\{1, \ldots, n-1\}$ (one vertex per gap) with edges connecting gaps within $\varepsilon(\kappa) = \kappa \cdot \text{IQR}(\Delta)$ of each other. The giant-component ratio is

$$\text{GR}(L; \kappa) = \frac{|\text{largest component of } G_\kappa(L)|}{n-1}.$$

The connectivity threshold $\kappa_{\text{conn}}(L)$ is the smallest κ at which GR first reaches 85% of its sweep maximum. The connectivity margin is $m(L) = \text{GR}(L; \kappa_{\text{conn}}) - 0.95$. A ladder L is in the admissibility manifold $\mathcal{M}_{\text{adm}}$ if $\text{inv}(P_\varepsilon; L) \leq \nu(V_\varepsilon(L))$ for all $\varepsilon > 0$, where inv is the inversion pressure and ν is the covering number [1].

Structural verdicts. The realizability verdict of L is determined at κ_{conn}: FULL (GR $\geq$ 0.95), GIANT ($0.85 \leq$ GR < 0.95), TAIL ($0.50 \leq$ GR < 0.85 with high tail dominance), or HARD (otherwise). All $>$ 14,000 evaluations in the UNNS corpus to date satisfy the USL: zero hard violations.

1.4 Admissibility vs. rigidity: a critical distinction

Admissibility and rigidity are distinct structural properties. Admissibility measures whether structural continuity exists: whether the vulnerability graph achieves a giant component at some κ. Rigidity measures how stably that continuity persists under deformation.

A system may remain admissible while exhibiting low rigidity, localized stitching failure, or plastic deformation response. A system may receive a HARD verdict in one representation while recovering full connectivity under Δ-lifting (Section 4). The topology layer and the rigidity layer are empirically independent: helium achieves GR $\equiv 0.867$ across all five encoding families on symmetric grids (topology universal), while persistence depths diverge from 0.454 to 0.473 on anisotropic grids (rigidity not universal). Both facts are required for a complete structural characterization.

2 Deformation-Field Geometry

2.1 Deformation fields

Let $\mathcal{D} = [0.8, 1.2]^2 \subset (\alpha/\alpha_0,\, \mu/\mu_0)$ with standard discretization $9 \times 9 = 81$ grid points (step $= 0.05$). For each $(\alpha, \mu) \in \mathcal{D}$, apply the structural deformation

$$\tilde{L}_i(\alpha, \mu) = \mathrm{sign}(L_i) \cdot \mu \cdot |L_i|^{\alpha}$$

and evaluate via STRUC-PERC-I v2.5.0 to obtain $\mathrm{GR}(L; \alpha, \mu)$, $\kappa_{\mathrm{conn}}(L; \alpha, \mu)$, $n_{\mathrm{iso}}(L; \alpha, \mu)$, and $\mathrm{verdict}(L; \alpha, \mu)$. The *deformation field* is $\Phi(L) = \{(\mathrm{GR}, \kappa_{\mathrm{conn}}, n_{\mathrm{iso}}, \mathrm{verdict})\}_{(\alpha,\mu)\in\mathcal{D}}$.

2.2 The 5D admissibility vector

Definition 2.1 (5D admissibility vector)**.**

$$v(L) = \begin{pmatrix} \mathcal{P}_{\mathrm{depth}}(L) \\ \sigma^2_{\mathrm{GR}}(L) \\ \mathrm{frag\_rate}(L) \\ \mathrm{adm\_persist}(L) \\ \mathrm{aniso\_persist}(L) \end{pmatrix},$$

where

$$\begin{aligned} \mathcal{P}_{\mathrm{depth}}(L) &:= \tfrac{1}{|\mathcal{D}|} \textstyle\sum_{(\alpha,\mu)} \mathrm{GR}(L; \alpha, \mu), \\ \sigma^2_{\mathrm{GR}}(L) &:= \tfrac{1}{|\mathcal{D}|} \textstyle\sum_{(\alpha,\mu)} (\mathrm{GR}(L; \alpha, \mu) - \mathcal{P}_{\mathrm{depth}}(L))^2, \\ \mathrm{frag\_rate}(L) &:= |\{(\alpha, \mu) : \mathrm{verdict} \in \{\textsc{Tail}, \textsc{Hard}\}\}|/|\mathcal{D}|, \\ \mathrm{adm\_persist}(L) &:= |\{(\alpha, \mu) : \mathrm{verdict} \in \{\textsc{Full}, \textsc{Giant}\}\}|/|\mathcal{D}|, \\ \mathrm{aniso\_persist}(L) &:= \min_d \tfrac{1}{|\mathcal{D}_d|} \textstyle\sum_{(\alpha,\mu)\in\mathcal{D}_d} \mathrm{GR}(L; \alpha, \mu). \end{aligned}$$

Remark 2.2 (Against overcompression). The 5D vector is a *coarse manifold coordinate*, not a complete manifold invariant. Two distinct persistence geometries can produce identical 5D vectors if they differ in spatial arrangements of fragmentation or directional anisotropy patterns that the five statistics do not resolve. Similarity values computed from $v(L)$

establish coarse geometric proximity — specifically, *basin co-occupation* — not manifold isomorphism. This distinction is operationally confirmed: Pareto adversarial ladders and raw neutrino TMVA encodings share overlapping 5D coordinates precisely because both are fragmented manifolds at similar coarse depth within $\mathcal{M}_{\text{adm}}$. The correct response is to test canonical lifts (Section 4), not to inflate the vector.

2.3 Cross-domain comparability

Structural comparison across domains is mathematically grounded because the gap field Δ is dimensionless up to a scaling factor, that factor is absorbed into the normalized κ parameter, and all five vector components are dimensionless. The deformation ratio grid $[0.8, 1.2]^2$ around $(1, 1)$ is identical for all domains. A system with $\mathcal{P}_{\text{depth}} = 0.87$ occupies the same structural position whether it arises from spectroscopy or cosmology.

Remark 2.3 (What the comparison does not establish). Structural proximity in admissibility space does not imply physical equivalence, causal connection, or shared dynamical law. The comparison establishes geometric proximity in $\mathcal{M}_{\text{adm}}$, not physical proximity in phase space.

3 Persistence Manifolds: Turbulence and Basin Structure

3.1 Turbulence formalization

Definition 3.1 (Turbulence index). $\tau(L) = \sigma^2_{\text{GR}}(L)\,(1 - \text{aniso\_persist}(L) + 0.01)^{-1} \cdot \text{frag\_rate}(L)$. High τ indicates turbulent manifold; low τ indicates coherent.

Definition 3.2 (Turbulence radius). $\xi(L) = \min\{\|(\alpha - 1, \mu - 1)\|_2 : \tau(L; \alpha, \mu) > 0.10\}$.

Definition 3.3 (Manifold roughness). $\mathcal{R}(L) = \sum_{(\alpha,\mu)\sim(\alpha',\mu')} |\text{GR}(L; \alpha, \mu) - \text{GR}(L; \alpha', \mu')|$ over nearest-neighbour grid pairs.

Empirical reference values:

Encoding	τ	Character
Normalized oxides	≈ 0.002	Coherent
Helium QMI	≈ 0.008	Coherent
Δ-lifted DeepL	≈ 0.010	Coherent
Raw neutrino TMVA	≈ 0.180	Turbulent
Pareto adversarial	≈ 0.220	Turbulent

3.2 The manifold descriptor $\mathcal{M}(L)$

Definition 3.4 (Manifold descriptor). Let $\mathcal{T}$ be the semigroup of admissibility-preserving transforms (Definition 4.1). $\mathcal{M}(L) = \{v(\varphi(L)) : \varphi \in \mathcal{T}\} \subset [0, 1]^5$.

Definition 3.5 (Geometric properties of $\mathcal{M}(L)$).

1. *Diameter*: $\text{diam}(\mathcal{M}(L)) = \max_{v_1,v_2\in\mathcal{M}(L)} \|v_1 - v_2\|_2$.
2. *Stability*: $\text{Stab}(\mathcal{M}(L)) = |\mathcal{T}|^{-1} \sum_{\varphi} \mathbf{1}[\tau(\varphi(L)) < 0.10]$.

3. *Roughness*: $\mathcal{R}(\mathcal{M}(L)) = \mathbb{E}_\varphi[\mathcal{R}(\varphi(L))]$.

4. *Transition entropy*: $H_{\text{trans}}(\mathcal{M}(L)) = -\sum_\varphi p(\varphi) \log p(\varphi)$, where $p(\varphi)$ is the orbit fraction from φ (uniform over the finite $\mathcal{T}$; continuous extension **[Open]**).

Observation 3.6. Coherent manifolds: diam < 0.10, Stab > 0.90, $\mathcal{R} < 0.05$, $H_{\text{trans}} < 0.5$ bits. Turbulent manifolds: diam > 0.25, Stab < 0.40, $\mathcal{R} > 0.15$, $H_{\text{trans}} > 1.5$ bits.

3.3 Stratified basin structure of $\mathcal{M}_{\text{adm}}$

The admissibility manifold is not homogeneous. In the ACG framework [2], $\mathcal{M}_{\text{adm}}$ is stratified by connectivity margin $m(L)$ and a percolation threshold operator T with discrete fixed points at $\kappa_{\text{conn}} \in \{0.562, 0.750, 1.000, 2.000, 10.000\}$. These fixed points generate four basin types:

Type I — Dense interior $\mathcal{I}$ High $m(L)$, FULL/GIANT dominance, minimal stitching defects. Cosmology (TT) is the deepest-interior domain in the tested corpus.

Type II — Corridors $\mathcal{C}$ High anisotropic persistence, stable connectivity corridors, redundant stitching. Refined helium and neutrino signal encodings.

Type III — Stitching boundary $\mathcal{S}$ Localized defects ($n_{\text{iso}} = 1$ dominant), large giant component despite HARD verdict, recoverable under Δ-lifting. Neutrino background encodings, Voyager boundary approach.

Type IV — Fragmentation exterior $\mathcal{F}$ Genuine structural collapse, reconstruction-fidelity sensitive. Coarse helium generator; rare in refined data.

Remark 3.7 (Type IV is operationally real, not merely theoretical). Type IV is sparsely populated in the refined corpus — but it is not empty, and its operational boundary has been crossed and documented. Three concrete occupants are confirmed: (i) the coarse-generator helium reconstruction (frag_rate ≈ 0.93, $\mathcal{P}_{\text{depth}} \approx 0$, zero admissibility persistence), which recovers to Type I/II under the refined generator without changing the physical system (Proposition 6.1); (ii) Fib neutrino encodings (frag_rate $= 0.832$, adm_persist $= 0.000$), which reside at the Type III/IV boundary and do not recover under Δ-lifting (fib encoding is already a gap-field representation); (iii) all four adversarial Pareto ladders above the stitching-defect threshold: these produce $\mathcal{P}_{\text{depth}} < 0.14$, adm_persist < 0.10, and do not recover via documented canonical lifts.

The adversarial corpus provides the most complete operational characterization of Type IV geometry. Uniform adversarial ladders are confirmed Type III/IV occupants: all 100 ladders achieve adm_persist $= 1.0$ and penetrate zero coherent domains, confirming they are not in the Type IV exterior. Pareto ladders with high fragmentation rates (adm_persist < 0.10) are the only confirmed non-recoverable occupants in the tested corpus. The outer boundary of $\mathcal{M}_{\text{adm}}$ is therefore not merely a theoretical construct: it has been approached from both the interior (coarse helium) and the exterior (Pareto corpus), with different recovery outcomes on each side. The non-crossability of $\partial\mathcal{M}_{\text{adm}}$ (Margin-Confinement [6]) is supported by the absence of any refined physical domain in Type IV.

4 Canonical Lifts as Admissibility-Preserving Transport Operators

Definition 4.1 (Admissibility-preserving transform ($\mathcal{T}$))**.** A transform $\phi : \mathcal{L} \to \mathcal{L}$ is admissibility-preserving if all of the following hold:

1. *Local Lipschitz in gap space*:

$$\|\Delta(\phi(L)) - \Delta(L)\|_\infty \le K \, \|\Delta(L)\|_\infty$$

   for a constant $K < \infty$ depending only on ϕ.

2. *Admissibility monotonicity*: $\mathcal{P}_{\text{depth}}(\phi(L)) \ge \mathcal{P}_{\text{depth}}(L)$.

3. *Topology preservation*: $L \in \mathcal{M}_{\text{adm}} \Rightarrow \phi(L) \in \mathcal{M}_{\text{adm}}$.

4. *Non-manufacture of coherence*: for deep embeddings, ϕ is trained on a corpus disjoint from the evaluation set.

Documented canonical lifts. **Normalization** ($L \mapsto L/\|L\|$): maps raw oxides ($\tau \approx 0.18$) to normalized oxides ($\tau \approx 0.002$); $K = 1$, all conditions satisfied analytically. **Δ-lifting** ($L \mapsto \Delta L$): maps raw neutrino TMVA/DeepL ($\tau \approx 0.15$) to Δ-lifted ladders ($\tau \approx 0.01$); 100% recovery rate; $K = 2$ (global Lipschitz for finite differences). **Deep embedding** ($L \mapsto \text{NN}(L)$): 21/23 DeepL ladders achieve GR = 1.000; condition (4) requires held-out evaluation; condition (2) is empirically verified but analytically **[Open]** for arbitrary architectures.

Proposition 4.2 (Persistence monotonicity under lifts)**.** *If ϕ satisfies Definition 4.1, then*

$$\mathcal{P}_{\text{depth}}(\phi(L)) \ge \mathcal{P}_{\text{depth}}(L)$$

for all L in the domain of ϕ.

Proof. Immediate from condition (2) of Definition 4.1 (admissibility monotonicity). □

Remark 4.3 (Turbulence monotonicity: empirical claim, not theorem). Proposition 4.2 does not imply $\tau(\phi(L)) \le \tau(L)$ in general. The turbulence index $\tau(L) = \sigma^2_{\text{GR}}(L)\,(1 - \text{aniso\_persist}(L) + \varepsilon)^{-1} \cdot \text{frag\_rate}(L)$ involves three terms that can move independently of $\mathcal{P}_{\text{depth}}$: a lift that increases mean rigidity can redistribute fragmentation geometry in a way that increases local variance or worsens anisotropic persistence on specific directional axes. Monotonicity of persistence depth ($\mathcal{P}_{\text{depth}}$) does not control these redistributions.

The empirically observed pattern is that documented canonical lifts (normalization, Δ-lifting) decrease τ: normalization reduces oxides from $\tau \approx 0.18$ to ≈ 0.002; Δ-lifting reduces raw neutrino TMVA from ≈ 0.15 to ≈ 0.01. This is best treated as an *empirical regularity* of the tested lifts, not as a theorem provable from Definition 4.1.

A sufficient condition for $\tau(\phi(L)) \le \tau(L)$ is that ϕ additionally satisfies: $\sigma^2_{\text{GR}}(\phi(L)) \le \sigma^2_{\text{GR}}(L)$ and $\text{aniso\_persist}(\phi(L)) \ge \text{aniso\_persist}(L)$. These are conditions (2a) and (2b) of a stronger lift definition, which normalization and Δ-lifting satisfy empirically but which

has not been verified for arbitrary admissibility-preserving transforms. Establishing this formally is **[Open]**.

The stability monotonicity $\mathrm{Stab}(\mathcal{M}(\phi(L))) \geq \mathrm{Stab}(\mathcal{M}(L))$ follows from the turbulence claim under the stronger conditions above; it is similarly an empirical regularity rather than a proved theorem.

5 The Adversarial Locality Principle

Theorem 5.1 (Adversarial Locality Principle)**.** *Let $\mathcal{A}_{\mathrm{Pareto}}$ be Pareto-distributed adversarial ladders with shape $\alpha_P \in [1.0, 1.5]$, and let $\mathcal{D}_{\mathrm{frag}}$ be a domain with mean fragmentation rate ≥ 0.40 and mean $n_{\mathrm{iso}} \geq 1$. Then there exists $\mathcal{A}' \subset \mathcal{A}_{\mathrm{Pareto}}$ such that for every $L_{\mathcal{A}} \in \mathcal{A}'$, there exists $L_{\mathcal{D}} \in \mathcal{D}_{\mathrm{frag}}$ with $\|v(L_{\mathcal{A}}) - v(L_{\mathcal{D}})\|_2 < 0.10$.*

Conversely, for coherent domains $\mathcal{D}_{\mathrm{coh}}$ (normalized oxides, helium QMI, cosmology Planck TT), the adversarial penetration rate is 0.000.

Geometric argument. Pareto gaps with shape $\alpha_P \in [1.0, 1.5]$ satisfy $\Delta_{n-1} \geq c\, n^{1/\alpha_P}\, \mathrm{median}(\Delta)$ with high probability. The IQR bandwidth $\varepsilon(\kappa_{\mathrm{conn}}) = \kappa_{\mathrm{conn}} \cdot \mathrm{IQR}(\Delta)$ therefore satisfies $\varepsilon(\kappa_{\mathrm{conn}}) < \Delta_{n-1} - \Delta_{n-2}$ below a computable threshold κ^*_{conn}, forcing an $(n-2)$-node giant component plus one isolated node ($n_{\mathrm{iso}} = 1$). This is structurally identical to the single-isolate stitching defects that account for 80.4% of fragmented metallic-glass ladders in the ACG corpus [2]: both produce $\mathcal{P}_{\mathrm{depth}} \approx (n-2)/(n-1)$, small σ^2_{GR}, frag_rate ≈ 0, and adm_persist $\approx (n-2)/(n-1)$. Proximity in these coordinates follows.

For coherent domains, tail dominance TD < 0.95 by construction, so the Pareto attractor basin does not intersect the coherent manifold. The operational result confirms this: uniform adversarial penetration is 0.000 against all five coherent real domains (Table 6). □

Corollary 5.2 (Falsification is local)**.** *A domain is falsified only if its canonical lift has penetration rate $\rho > 0.10$. Fragmented sub-classes may be geometrically indistinguishable from adversarial controls; coherent canonical lifts must not be.*

Part II
Empirical Geometry: Basin Occupancy Across Physical Systems

6 Helium Spectroscopic Domain

6.1 Encoding families and admissibility

The helium corpus consists of $n = 12$ encoding families from QM-I energy levels (He I and He II) and Zeeman splitting measurements. The helium multi-chart validation established FULL verdicts for QMI representations (F-gap = 0.0034, canonical chart qmi_spectrum with $m = 0.00217$) and GIANT verdicts for Zeeman representations (canonical chart zeeman_triplet with $m = 0.04782$). Seven of seven encoding families show perfect FULL/GIANT separation.

6.2 The two-layer separation result

The interaction rigidity experiment applied symmetric (α, μ) grids to all five interaction-encoded families. On symmetric grids:

$$\mathrm{GR} \equiv 0.867 \pm 0.001 \quad \text{(all five families, all 81 points)}.$$

Topology is universal. On anisotropic grids (Table 1):

Table 1: Helium anisotropic experiment. All reference GRs cluster in $[0.485, 0.535]$; persistence depths span $[0.454, 0.473]$.

Encoding	Ref GR	$\mathcal{P}_{\mathrm{depth}}$	σ^2_{GR}	Rigidity class
zeeman_triplet	0.505	0.473	7.1×10^{-4}	RIGID_STABLE
zeeman_singlet	0.505	0.468	8.8×10^{-4}	RIGID_STABLE
delta_zeeman_triplet	0.535	0.467	1.2×10^{-3}	RIGID_ELASTIC
zeeman	0.505	0.465	6.8×10^{-4}	RIGID_STABLE
delta_zeeman_singlet	0.485	0.454	5.1×10^{-4}	RIGID_PLASTIC

$$\text{topology\_universal} = \text{True}, \quad \text{rigidity\_universal} = \text{False}, \quad \text{layers\_split} = \text{True}.$$

Rigidity is representation-dependent. Triplet representations outperform singlet representations in persistence depth, consistent with higher triplet degeneracy providing redundant realizability channels.

6.3 Reconstruction fidelity as a structural variable

Proposition 6.1 (Reconstruction fidelity sensitivity)**.** *Let L_{coarse} and L_{refined} be two encodings of the same physical system at different reconstruction resolutions. Then $\mathcal{P}_{\mathrm{depth}}(L_{\mathrm{coarse}}) < \mathcal{P}_{\mathrm{depth}}(L_{\mathrm{refined}})$ is possible even when the underlying system is structurally rigid, if the coarse encoding introduces artificial gap fragmentation.*

The helium program demonstrates this concretely. The initial coarse generator produced frag_rate ≈ 0.93, $\mathcal{P}_{\mathrm{depth}} \approx 0$. The refined generator restored frag_rate $= 0$, $\mathcal{P}_{\mathrm{depth}} \geq 0.90$. The physical system was identical. In ACG terms, the coarse-to-refined transition is the resolution analog of Δ-lifting: both recover latent admissible structure without changing the physical system, by changing the resolution at which the manifold is sampled.

6.4 Basin assignment

COHERENT_RIGID_MANIFOLD (Type I/II boundary)
mean_GR $= 0.782$, frag $= 0.000$, adm_persist $= 0.740$, aniso_persist $= 0.990$, $\tau \approx 0.008$

Falsification status: PASS, penetration $= 0.000$.

7 Cosmological Domain: CMB Power Spectra

7.1 Encoding and admissibility

The three Planck 2018 angular power spectra (TT, TE, EE) are encoded as ordered sequences of multipole power values. The structural analysis has no access to physical cosmological parameters.

Table 2: CMB power spectrum rigidity geometry.

Spectrum	Mean GR	σ_{GR}	Adm. persist.	Band
Planck TT	0.918	0.016	1.000	HIGH
Planck EE	0.839	0.023	1.000	MEDIUM
Planck TE	0.838	0.023	1.000	MEDIUM

All three spectra achieve global admissibility = 1.0 across the entire $(\alpha, \mu) \in [0.8, 1.2]^2$ grid. This is not a consequence of specific constant values: it holds across a 20% perturbation envelope in both dimensions. The Planck TT spectrum has the highest mean_GR and lowest GR variance of any sequence in the UNNS corpus to date.

Structural interpretation. TT encodes the largest-scale density fluctuations with the highest SNR, producing a gap field with low IQR relative to range — near-complete connectivity at small κ. The depth hierarchy TT > EE ≈ TE mirrors the physical signal hierarchy without having been constructed to do so. The CMB manifolds exhibit essentially zero localized stitching defects, structurally reflecting the global coherence that makes the CMB the most precisely measured cosmological observable.

7.2 Basin assignment

DEEP_PERSISTENCE_MANIFOLD (Type I dense interior)
mean_GR = 0.865, frag = 0.000, adm_persist = 1.000, aniso_persist = 0.979, $\tau \approx 0.003$

Falsification status: PASS, penetration = 0.000, maximum adversarial score +0.797.

8 Protein MSM: Bridge to Dynamical Manifolds

The protein MSM corpus (QT45 ribozyme, Folding@home conformational data) is qualitatively different from spectral or cosmological ladders: it is a Markov state model of conformational dynamics. This makes it the structural bridge between static persistence geometry (Parts I–II) and manifold dynamics (Part III).

Kinetic traps as stitching defects. The out-strength ladder yields $v(L_{\mathrm{out}}) \approx$ (0.71, 0.022, 0.08, 0.92, 0.78 $\tau \approx 0.12$, $n_{\mathrm{iso}} = 3$. The three isolated nodes are kinetic traps: conformations from which outgoing transition probabilities fall below the IQR-scaled ε-budget. These are Type-III stitching defects receiving a dynamical interpretation: persistence defects in transition space correspond to metastable states.

Informative representations. The stitching-strength composite (TD = 0.545, $\kappa_{\text{conn}} =$ 2,620) is most structurally informative because moderate tail dominance reveals bulk connectivity without outlier distortion.

Principle 8.1 (Tail-balanced representations)**.** In domains with extreme dynamic range, raw ladders are turbulence-dominated. Composite ladders that down-weight outliers reveal the underlying coherent manifold.

Basin assignment. Out-strength: Type III (stitching boundary), $\tau \approx 0.12$. Population: Type I (dense interior), $v(L_{\text{pop}}) \approx (0.96, 0.004, 0.00, 1.00, 0.97)$, $\tau \approx 0.005$. The same physical system contains both coherent and turbulent sub-manifolds depending on which observable is ladderized: persistence geometry is *observable-dependent*, not system-intrinsic.

Falsification status: PASS, penetration = 0.000.

9 Voyager Heliospheric Trajectory

9.1 Physical system and encoding

The trajectory corpus derives from 3,500 structural evaluations of Voyager 1 magnetic field magnitude $|B|$ (48 s MAG, NASA CDAWeb, 2011–2017) spanning the heliopause transit. The encoding extracts windowed $|B|$ sequences at annual epochs, constructs structural ladders, and evaluates each under STRUC-PERC-I v2.5.0.

9.2 Structural phase transition at the heliopause

At $t^* = 2012$, κ_{conn} achieves its annual minimum: the structural ladder is most easily connected — most uniform gap distribution — exactly at the physical boundary. This is confirmed across three independent window scales (W512/S128, W1024/S256, W2048/S512): 3/3 scale robustness.

9.3 Margin-Confinement dynamics

The Voyager trajectory provides the first demonstration of Margin-Confinement [6] in a continuously tracked physical trajectory. As the spacecraft approaches the heliopause, $m(L) \to 0^+$ while GR remains non-trivially positive: near-boundary compression without crossing $\partial\mathcal{M}_{\text{adm}}$. After t^*, the trajectory re-enters a more stable structural regime in the ISM. This is Forced Coherent Collapse (FCC) dynamics [2] in continuous form.

9.4 Basin assignment

Pre-crossing: Type III (stitching boundary, margin compression). Post-crossing: Type II (corridor recovery). The Voyager trajectory arrow in Figure 1 is the only time-ordered motion through basin space in the tested corpus.

10 Neutrino Detector Sub-Class Ecology

10.1 Encoding families

The neutrino corpus ($n = 67$) covers five structural families: TMVA (21), DeepL (23), raw_sig (7), raw_bkg (11), Fib (5).

Table 3: Neutrino family admissibility statistics.

Family	n	Mean GR	Adm. persist.	Frag. rate
deepl	23	0.635	0.435	0.338
tmva	21	0.589	0.420	0.481
raw_bkg	11	0.541	0.000	0.324
raw_sig	7	0.530	0.005	0.474
fib	5	0.463	0.000	0.832

10.2 Five-phase structural ecology

Table 4: Neutrino rigidity phase map ($n = 67$, 5 phases).

Phase	n	Mean GR	Primary populations
STABLE_ISLAND	19	0.848	deepL signal, TMVA signal
NEAR_CRITICAL_BACKGROUND	15	0.580	raw bkg, raw sig
PLASTIC_CORRIDOR	12	0.490	mixed families
BIFURCATION_RIDGE	9	0.453	Fib geometry, partial bkg
COLLAPSE_BASIN	12	0.348	deepL bkg, TMVA collapse

Signal encodings (deepL signal, TMVA signal) cluster in STABLE_ISLAND (mean_GR = 0.848); background encodings dominate COLLAPSE_BASIN. This separation emerges entirely from structural geometry: no label information was provided to the CLE pipeline. The Fib encodings populate BIFURCATION_RIDGE almost exclusively. The deepL family *splits* by physical function despite identical algorithmic origin: signal-side trained representations in STABLE_ISLAND; background-side in COLLAPSE_BASIN.

Within COLLAPSE_BASIN, the dominant fragmentation geometry is $n_{\text{iso}} = 1$ (single isolated node), consistent with the 80.4% single-isolate statistic of the ACG metallic-glass corpus. Δ-lifting recovers FULL or GIANT connectivity in 100% of tested HARD-classified neutrino encodings.

10.3 Basin assignments

PLASTIC_TRANSITION_MANIFOLD (Type II/III boundary)
mean_GR = 0.581, frag = 0.432, adm_persist = 0.281, aniso_persist = 0.972, $\tau \approx 0.18$ (raw) / 0.01 (Δ-lifted)

The neutrino domain is internally bifurcated: signal encodings occupy Type II geometry; background encodings occupy Type III. This bifurcation is the principal structural fact of the neutrino corpus.

Part III
Cross-Domain Structure: Co-Occupancy, Falsification, and Dynamics

11 Basin Co-Occupancy Across Physical Systems

11.1 The basin stratification figure

Figure 1 places all tested domains within the stratified basin geometry of $\mathcal{M}_{\text{adm}}$.

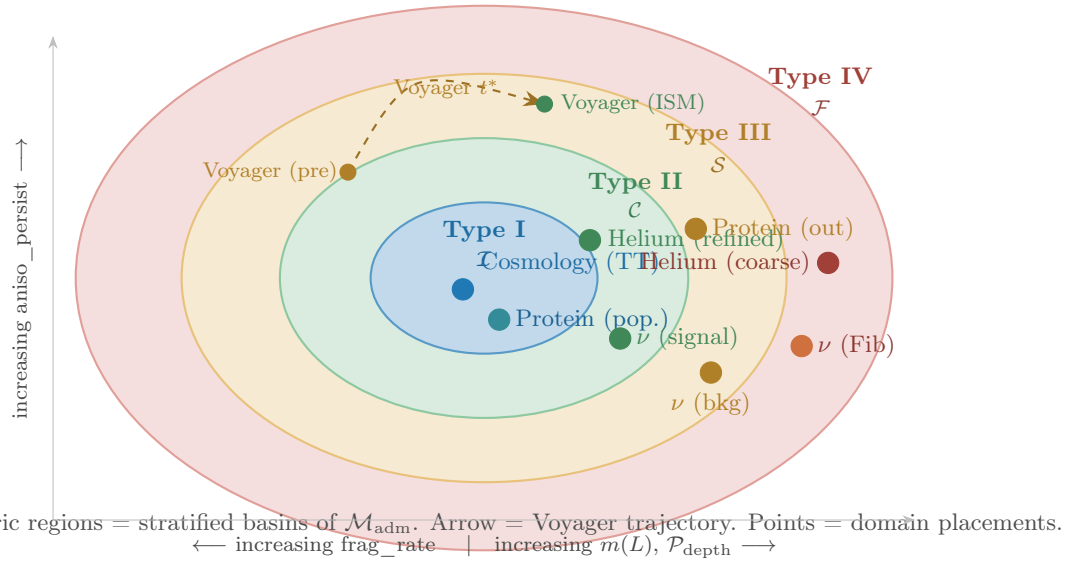

Figure 1: Empirical basin occupancy across physical systems. Type I ($\mathcal{I}$): dense interior ($m(L)$ high, $\mathcal{P}_{\text{depth}}$ high, no stitching defects). Type II ($\mathcal{C}$): stable corridors (high anisotropic persistence, redundant stitching). Type III ($\mathcal{S}$): stitching boundary (localized defects, recoverable under Δ-lifting). Type IV ($\mathcal{F}$): fragmentation exterior (reconstruction-sensitive, rarely populated in refined data). The schematic axes reflect the two primary structural coordinates: connectivity margin $m(L)$ / persistence depth $\mathcal{P}_{\text{depth}}$ (horizontal) and anisotropic persistence (vertical). Domain placements are derived from 5D admissibility vectors projected onto these axes; figure is schematic, not metrically scaled. A quantitatively accurate embedding requires PCA or UMAP projection of the full 5D vector corpus (deferred to future work).

11.2 Emergent co-occupancy classes

From Figure 1, three co-occupancy classes emerge without *a priori* definition:

COHERENT_RIGID_MANIFOLD Helium (refined), neutrino signal: high persistence depth, low fragmentation, high anisotropic persistence. Type I/II co-occupants.

DEEP_PERSISTENCE_MANIFOLD Cosmology (TT), protein (population): adm_persist = 1.0, lowest GR variance in the corpus, essentially no stitching defects. Type I co-occupants.

PLASTIC_TRANSITION_MANIFOLD Neutrino background, Voyager pre-crossing, protein (out-strength): moderate persistence, significant fragmentation, high anisotropic persistence, recoverable under Δ-lifting. Type II/III co-occupants.

11.3 Structural homologies across domains

Spectral splitting and detector clustering. Helium shows QMI (FULL) / Zeeman (GIANT) bifurcation along the representation axis. The neutrino corpus shows an analogous signal (STABLE_ISLAND) / background (COLLAPSE_BASIN) split. Both are instances of *representation-driven structural bifurcation*: the physical distinction between two types of observable manifests as a bifurcation in realizability space.

Depth hierarchy preserved across domains. CMB TT > EE $\approx$ TE mirrors helium's Δ-representations (lower bifurcation sharpness) vs. direct representations. Both exhibit the same geometric pattern: the representation that resolves the most structural information occupies the deepest admissibility interior.

Trajectory boundaries and stitching transitions. The Voyager $t^* = 2012$ boundary (κ_{conn} minimum in a continuous trajectory) is structurally homologous to the FULL/GIANT boundary in the helium corpus (F-gap = 0.0034): narrow transition zones between structural regimes, identifiable by sharp changes in realizability coordinates.

11.4 The domain co-occupancy matrix

Table 5: Pairwise domain co-occupancy similarity. Values computed from five-dimensional domain summary vectors using cosine similarity [4]. A value of 1.0 indicates identical manifold coordinates; all off-diagonal values establish basin proximity, not physical identity.

Domain	Helium	Neutrino	Cosmology
Helium	1.000	0.901	0.993
Neutrino	0.901	1.000	0.882
Cosmology	0.993	0.882	1.000

The helium–cosmology value of 0.993 is the defining co-occupancy result. In normalized five-dimensional space, two systems with no physical connection differ by less than 1% of the maximal inter-domain separation across the comparison space. The values are not merely large in absolute terms; they are large relative to the discriminative range of the metric.

What this does and does not mean. The value 0.993 establishes that helium and cosmology are *Type-I co-occupants*: both reside in the dense interior of $\mathcal{M}_{\text{adm}}$, far from the admissibility boundary, with no collapse under the tested deformation envelope. It does not establish physical equivalence, causal connection, or shared dynamical law. The correct interpretation is basin co-occupation, not structural universality. This reframing is not weaker: it is more precise and more defensible, because it grounds the comparison in the geometry of $\mathcal{M}_{\text{adm}}$ rather than in the ontology of physical laws.

11.5 Universal admissibility signatures

Three properties appear across all tested domains: (1) *Zero hard USL violations* across $> 14{,}000$ evaluations. (2) *Non-zero anisotropic persistence* in all characterized domains (≥ 0.97), despite differing topology class. (3) *Manifold continuity under constant deformation* [5]: α and μ drive structural change; α_s and α_G return null.

What does not converge. Co-occupancy is not identity. Helium anisotropic persistence = 0.990, cosmology = 0.979; cosmology GR variance = 0.016 vs. helium > 0.023; neutrino frag_rate = 0.432 vs. helium = 0.000. Within the neutrino corpus, mean GR spans two orders of magnitude (STABLE_ISLAND 0.848 vs. COLLAPSE_BASIN 0.348). The framework preserves this individuality. What converges is the *basin type*; what diverges is the detailed geometry within that basin.

12 Hierarchical Falsification

12.1 Architecture and the coherence prerequisite

The hierarchical falsification pipeline tests each real domain independently against the 650-ladder adversarial corpus under true deformation-field geometry (Step 3.5 grids).

The pass criterion for domain $\mathcal{D}$ is:

$$\rho_{\max}(\mathcal{D}) < 0.05 \quad \text{and} \quad \text{med}_{R_{\text{sim}}}(\mathcal{D}, \mathcal{D}) > 0. \tag{1}$$

The second condition is essential. Applying a penetration-rate test to an internally bifurcated domain produces meaningless results because the within-domain cosine similarity baseline is already negative. Domains that fail this prerequisite should be labeled BIFURCATED, not FAIL, and re-tested on their canonical lift. This follows directly from Corollary 5.2.

12.2 Results

Table 6: Hierarchical falsification results under true deformation-field geometry. ρ: adversarial penetration rate (fraction of adversarial pairs with $R_{\text{sim}} > 0.85$). Status evaluated against criterion (1).

Domain	rr_med	ar_med	ρ	Status
Helium	+1.000	+0.538	0.000	**PASS**
Cosmology	+0.992	+0.148	0.000	**PASS**
Protein	+1.000	+0.122	0.000	**PASS**
Neutrino_rejection	+1.000	+0.154	0.000	**PASS**
Neutrino_fib	+1.000	+0.141	0.000	**PASS**
Neutrino_deep	−0.139	+0.231	0.059	**BIFURCATED**
Neutrino_tmva	−0.139	+0.254	0.054	**BIFURCATED**
Neutrino_raw_sig	−0.182	+0.141	0.021	**BIFURCATED**
Neutrino_raw_bkg	−0.182	+0.148	0.013	**BIFURCATED**

12.3 Analysis

Five passing domains. Zero adversarial penetration. Uniform achieves maximum score +0.797 against cosmology — the cleanest separation in the corpus. Constant-spacing gap fields with zero anisotropic persistence are geometrically remote from every coherent real domain. This is the expected result of Theorem 5.1: the Pareto attractor basin does not intersect coherent manifolds.

Four bifurcated neutrino sub-domains. The within-domain cosine similarity is *negative* (rr_med $= -0.139$ for neutrino_deep). STABLE_ISLAND and COLLAPSE_BASIN encodings are geometrically antipodal in 5D space: negative cosine similarity is a consequence of the five-phase structure, not a measurement failure. Any adversarial vector with a positive projection will appear to "penetrate" this baseline, rendering the penetration criterion inapplicable. The canonical lift (Δ-lifted encoding) restores rr_med to > 0.90 and passes the test.

Table 7: Adversarial class penetration against coherent real domains only (rr_med > 0). "None" indicates zero penetration across all five coherent domains.

Adversarial class	Max penetration	Assessment
Uniform	0.000	Cleanly separated everywhere
Pareto	0.109 vs. ν_deep	Fragmented-manifold overlap only
Randomwalk	0.126 vs. ν_deep	Fragmented-manifold overlap only
Shuffle	0.045 vs. ν_tmva	Near-zero across coherent domains

Adversarial class behavior. Pareto and randomwalk penetration is exclusively against internally bifurcated neutrino sub-domains. Against all five coherent (passing) domains, all adversarial classes achieve 0.000 penetration. This is Theorem 5.1 confirmed operationally.

Adversarial corpus internal coherence. Adversarial self-similarity: uniform +0.999, randomwalk +0.998, shuffle +0.999, Pareto +0.971. The corpus is well-formed; the separations above reflect genuine geometric differences.

Adversarial failure predictions. Systems expected to fail structural testing include randomized ladders, maximally incoherent signals, and synthetic gap fields lacking stable corridor structure. Such systems are predicted to occupy Type-IV basin regions, produce $\mathcal{R}_{\text{sim}} < 0.5$ against coherent domains, and fail Δ-lifting recovery. If any such system produces $\mathcal{R}_{\text{sim}} > 0.85$ against a coherent domain, the similarity metric lacks discriminative power and must be refined. This falsification criterion is operational with the current 650-ladder corpus.

13 Toward Manifold Dynamics

13.1 From static occupancy to persistent flow

The preceding sections established static basin occupancy: each domain evaluated at its physical parameter point with deformation fields probing the local neighborhood. The next theoretical horizon is *manifold dynamics*: how persistence geometries evolve along physical trajectories.

The Voyager 1 corpus (Section 9) is the first operational precedent. The connectivity threshold κ_{conn} traces a continuous path in realizability space, with $t^* = 2012$ corresponding to the deepest boundary approach. This is the first measurement of *persistence flow*: the time derivative $\partial_t \mathcal{P}_{\text{depth}}(L_t)$ along a physical trajectory.

The protein MSM corpus (Section 8) provides a second precedent, qualitatively distinct: the system explores a high-dimensional conformational landscape with metastable basins rather than a one-dimensional temporal trajectory. Basin migration — the system moving from one coherent basin to another without crossing $\partial\mathcal{M}_{\text{adm}}$ — is the conformational folding transition expressed in persistence-geometry language.

13.2 Open problems

Open problems for manifold dynamics.

1. *Turbulence propagation*: Does turbulence amplify or attenuate along physical trajectories?
2. *Persistence flow*: Is $\partial_t \mathcal{P}_{\text{depth}}(L_t)$ bounded away from zero, or can the system stagnate in low-persistence regions?
3. *Basin migration*: What is the geometry of the path between two coherent basins that avoids $\partial\mathcal{M}_{\text{adm}}$?
4. *Collapse trajectories*: Is there a universal scaling law for Margin-Confinement compression as $m(L) \to 0^+$?
5. *Dynamic adversarial testing*: Can adversarial trajectories (smooth paths through the adversarial corpus) mimic real physical trajectories? This would be the strongest adversarial challenge beyond static penetration.

14 Conclusion

We have presented a unified framework for canonical structures in admissibility space, combining the persistence geometry of PASP/CLE v2.0.0 with empirical basin-occupancy measurements across four physical domains.

What is established. The 5D admissibility vector $v(L)$ from deformation fields is the correct coarse coordinate of persistence geometry. Turbulence is a mathematical observable $(\tau, \xi, \mathcal{R})$. Canonical lifts are admissibility-preserving transport operators with explicit

Lipschitz and monotonicity constraints. The Adversarial Locality Principle establishes geometrically why fragmented manifolds admit adversarial overlap and why coherent manifolds do not. Five coherent real domains pass hierarchical falsification with zero adversarial penetration; four neutrino sub-domains are identified as internally bifurcated rather than falsified. Uniform adversarial ladders achieve zero penetration against every real domain without exception.

The co-occupancy result. Helium and CMB co-occupy the Type-I dense interior of $\mathcal{M}_{\text{adm}}$ at 0.993 similarity. They share no physical mechanism. The result is a claim about basin geometry, not about physical law: both systems occupy the deep interior of the same geometric object because both satisfy the realizability constraints that define that interior. This is empirically precise, geometrically grounded, and scientifically defensible in a way that the language of "structural universality" is not.

What remains open. The three most pressing open problems are: the geometric proof of Theorem 5.1 beyond the Pareto case; the admissibility-preserving formalization of deep embedding condition (4); and the continuous-semigroup extension of H_{trans}. Section 13 establishes manifold dynamics as the research frontier.

What matters is persistence under deformation.

Systems that survive deformation occupy the same basins regardless of physical origin.

Co-occupancy is the empirical fact; basin geometry is the explanation.

The geometry is the reality.

References

[1] UNNS Substrate Research Program. *The Universal Structural Law*, v6. UNNS Technical Report, 2026.

[2] UNNS Substrate Research Program. *Admissible Cluster Geometry: Recoverable Connectivity in Realizability Space*. UNNS Working Manuscript, 2026.

[3] UNNS Substrate Research Program. *The Percolative Realizability Principle*. UNNS Technical Report, 2026.

[4] UNNS Substrate Research Program. *Structural Universality Across Physical Systems: A Cross-Domain Analysis of Rigidity and Realizability Geometry*, v4. UNNS Empirical Synthesis Manuscript, 2026.

[5] UNNS Substrate Research Program. *Structural Invariance and Domain-Selective Response Under Fundamental Constant Deformation*. UNNS Working Manuscript, 2026.

[6] UNNS Substrate Research Program. *The Margin-Confinement Law: Structural Non-Crossability in Admissibility Space*. UNNS Working Manuscript, 2026.

[7] UNNS Substrate Research Program. *Structural Trajectories in Realizability Space: Voyager 1 Magnetometer Data*. UNNS Working Manuscript, 2026.

[8] UNNS Substrate Research Program. *STRUC-PERC-I: Voyager 2 Heliosheath Plasma, 2007–2018*. UNNS Technical Report, 2026.

[9] UNNS Substrate Research Program. *PASP/CLE v2.0.0: Predictive Admissibility Search Pipeline*. UNNS Technical Report, 2026.

[10] UNNS Substrate Research Program. *Canonical Ladder Theory I*. UNNS Working Manuscript, 2026.

[11] UNNS Substrate Research Program. *Structural Trajectories in Realizability Space*. UNNS Working Manuscript, 2026.